Cryo-EM structure of the benzodiazepine-sensitive α1β1γ2 heterotrimeric GABAA receptor in complex with GABA illuminates mechanism of receptor assembly and agonist binding

Swastik Phulera*[1], Hongtao Zhu*[1], Jie Yu*[1], Derek Claxton[1‡], Nate Yoder[1], Craig Yoshioka[1] and Eric Gouaux[1,2]

[1]Vollum Institute, Oregon Health and Science University; [2]Howard Hughes Medical Institute, Oregon Health and Science University, 3181 SW Sam Jackson Park Road, Portland OR 97239

‡ Present address: Department of Molecular Physiology and Biophysics, Vanderbilt University, 741 Light Hall 2215 Garland Avenue, Nashville TN 37232

*These authors contributed equally

Correspondence to Eric Gouaux: gouauxe@ohsu.edu

ABSTRACT

Inhibitory neurotransmission in the mammalian nervous system is largely mediated by $GABA_A$ receptors, chloride-selective members of the superfamily of pentameric Cys-loop receptors. Native $GABA_A$ receptors are heteromeric assemblies sensitive to a tremendous array of important drugs, from sedatives to anesthetics and anticonvulsive agents, and mutant forms of $GABA_A$ receptors are implicated in multiple neurological diseases, including epilepsy. Despite the profound importance of heteromeric $GABA_A$ receptors in neuroscience and medicine, they have proven recalcitrant to structure determination. Here we present the structure of the triheteromeric $\alpha1\beta1\gamma2$ $GABA_A$ receptor in complex with GABA, determined by single particle cryo-EM at 3.1-3.5 Å resolution. The structure elucidates the molecular principles of receptor assembly and agonist binding as well as showing how remarkable *N*-linked glycosylation on the α_1 subunit occludes the extracellular vestibule of the ion channel and is poised to modulate receptor gating and assembly. Our work provides a pathway to structural studies of heteromeric $GABA_A$ receptors and thus a framework for the rational design of novel therapeutic agents.

INTRODUCTION

$GABA_A$ receptors are chloride permeable, γ-amino butyric acid (GABA)-gated ion channels that are responsible for the majority of fast inhibitory neurotransmission in the mammalian nervous system (Sigel and Steinmann 2012). Because of the fundamental role that $GABA_A$ receptors play in balancing excitatory signaling, which is largely due to the activity of ionotropic glutamate receptors, $GABA_A$ receptors are central to the development and normal function of the central nervous system (Wu and Sun 2015). In accord with their crucial role in brain function, mutations in $GABA_A$ receptor genes are directly linked to epilepsy syndromes (Hirose 2014) and are associated with schizophrenia, autism, alcohol dependence, manic depression and eating disorder syndromes (Rudolph and Mohler 2014). Moreover, $GABA_A$ receptors are the targets of a large number of important therapeutic drugs, from sedatives, sleep aids and anticonvulsive medications to anesthetic agents (Braat and Kooy 2015). $GABA_A$ receptors are also the target of alcohol and are implicated in alcohol dependence (Trudell, Messing et al. 2014).

$GABA_A$ receptors belong to the pentameric ligand–gated ion channel (PLIGC) superfamily (Thompson, Lester et al. 2010). Other members of this family are nicotinic acetylcholine, 5-HT3, $GABA_A$, glycine, and the invertebrate GluCl and Zn^{2+} -activated cation channels (Thompson, Lester et al. 2010). Members of this family are composed of five protein subunits which together form a central ion pore. Each subunit contains four transmembrane domains (M1–M4) along with an extracellular N- and C- termini. $GABA_A$ receptors are typically found as heteropentameric channels derived from a pool of 19 possible subunits: α1–6, β1–3, γ1–3, δ, ε, θ, π, and ρ1–3 (Sigel and Steinmann 2012). A

vast number of possible subunits gives rise to a myriad of theoretically possible pentameric assemblies; Nevertheless, the most prevalent subunit combination in the vertebrate brain is considered to be composed of two α, two β and one γ (Chang, Wang et al. 1996, Tretter, Ehya et al. 1997, Farrar, Whiting et al. 1999) with the arrangement of subunits being β-α-β-γ–α, clockwise when viewed from the extracellular space (Baumann, Baur et al. 2001, Baumann, Bauer et al. 2002, Baur, Minier et al. 2006). The molecular basis for selective subunit assembly of $GABA_A$ receptors is not well understood.

Pioneering structural studies of the paradigmatic acetylcholine receptor (AChR) (Unwin 2005), as well as crystallographic studies of homomeric PLIGCs that include prokaryotic pLGICs (Hilf and Dutzler 2008) and the eukaryotic GluCl (Hibbs and Gouaux 2011), 5-HT3A serotonin receptor (Hassaine, Deluz et al. 2014), human β3 $GABA_A$ (Miller and Aricescu 2014), human α3 GlyR (Huang, Chen et al. 2015), along with cryo-electron microscopy structure of the zebrafish α1 glycine receptor (GlyR) (Du, Lu et al. 2015) and the human 5-HT3A receptor (Basak, Gicheru et al. 2018), have helped to shape our understanding of receptor architecture and mechanism. Recent structures of diheteromeric nAChRs (Walsh, Roh et al. 2018), also further our understanding of heteromer assembly.

These studies, together with a large number of biochemical and biophysical experiments, have defined the transmembrane, ion channel pore, its lining by the M2 helices and likely mechanisms of ion selectivity (Sine, Wang et al. 2010, Cymes and Grosman 2016). The extracellular N-terminal domain harbors the orthosteric agonist binding site, located at a subunit interfaces, in addition to multiple binding sites for an

array of small molecules or ions that act as allosteric modulators (Lynagh and Pless 2014). While the mechanism by which orthosteric agonists and competitive antagonists activate or inhibit ion channel activity is well explored (Gielen and Corringer 2018), the molecular mechanisms for the action of allosteric ligands, especially those that act on heteromeric $GABA_A$ receptors, remain to be fully elucidated. Here we present methods for the expression and isolation of triheteromeric $GABA_A$ receptors and the cryo-EM structure of the rat $\alpha1\beta1\gamma2$ $GABA_A$ receptor, thus defining subunit assembly, the mode of GABA binding to the orthosteric agonist binding site and the remarkable of *N*-linked glycosylation of the $\alpha1$ subunit.

Receptor expression and structure elucidation

To enhance receptor expression level, we employed the M3/M4 loop deletion constructs of the $\alpha1$ and $\beta1$ subunits analogous to the functional M3/M4 loop deletion constructs of GluCl (Hibbs and Gouaux 2011) and GlyR (Du, Lu et al. 2015), together with a full length construct of the $\gamma2$ subunit (Supplementary Figure 2). Optimization of receptor expression constructs and conditions was followed by fluorescence detection size exclusion chromatography (FSEC) (Kawate and Gouaux 2006). To selectivity isolate the triheteromeric complex, we included a 1D4 affinity tag (MacKenzie, Arendt et al. 1984) on the $\gamma2$ subunit, thus allowing us to isolate sufficient quantities of baculovirus transduced mammalian cells (Goehring, Lee et al. 2014) for biochemical and structural studies. For the ensuing cryo-EM studies, we isolated a $\alpha1$ subunit specific monoclonal antibody, 8E3, with the aim of using the Fab fragment to identify the $\alpha1$ subunit in the pseudo symmetric receptor complex (Supplementary Figure 1). The resulting purified receptor, in the presence of the 8E3 Fab, binds muscimol, a high affinity agonist, and flunitrazepam, a

benzodiazepine, with affinities similar to the full length receptor (Supplementary Figure 3) (Hauser, Wetzel et al. 1997, Johnston 2014). Moreover, the cryo-EM receptor construct also exhibits ion channel gating properties that are similar to the wild-type receptor in the presence and in the absence of Fab (Supplementary Figure 3) (Li, Eaton et al. 2013). We notice, however, that while the cryo-EM construct retains potentiation by diazepam, the extent of potentiation is reduced for the Fab complex.

Structure elucidation of the heterotrimeric complex was carried out using receptor solubilized in dodecylmaltoside and cholesterol hemisuccinate (CHS), in the presence of 1.5 mM GABA. To enhance particle density on the cryo-EM grids despite modest levels of receptor expression, we employed grids coated with graphene oxide. We proceeded to collect micrographs using a Titan Krios microscope and a Falcon 3 camera as described in the Material and Methods. Subsequent selection of particles and calculation of 2D class averages yielded projections that were readily identified as a pentameric Cys-loop receptor bound by 2 Fab fragments (Figure 1). Three dimensional reconstruction, followed by judicious masking of, alternatively, the Fab constant domains or the receptor transmembrane domain (TMD) allowed for reconstructions at ~3.5 Å and ~2.7 Å resolution, respectively, based on Fourier Shell Correlation (FSC) analysis (Table 1). Inspection of the resulting density maps were consistent with these resolution estimations, and in the case of the density in the extracellular domain (ECD), the quality of the density map is excellent, allowing for visualization of many medium and large side chains, as well as glycosylation of Asn side chains. By contrast, the density for the TMD is not as well defined. While the M1, M2 and M3 helices of all subunits have strong density, with characteristic corkscrew shape and appearance of some large side chains,

the M4 helices of the two α1 subunits and the γ subunit have weak density and thus their positions are tentative. For the remainder of the complex, we first generated homology models of the α1, β1 and γ2 subunits using the homomeric $GABA_A$ receptor as a template, manually fit the models to the density and carried out iterative cycles of manual fitting and computational refinement, which together resulted in a structural model that fits well to the density and that has good stereochemistry (Supplementary Table 1).

Heterotrimeric $GABA_A$ receptor subunit arrangement

The α1β1γ2 receptor hews to the classic architecture of Cys-loop receptors, first established by cryo-EM studies of the nicotinic receptor (Toyoshima and Unwin 1988, Unwin 1993, Unwin 2005), with a clockwise subunit arrangement of α1-β1*-γ2-α1*-β1 when viewing the receptor from extracellular side of the membrane. Here we label the α1* and β1* subunits that are adjacent to the unique γ2 subunit with asterisks in order to distinguish them from their chemically equivalent yet spatially distinct α1 and β1 partners. The arrangement of subunits in this heteromeric complex, as mapped out by the α1-binding Fab fragments is in agreement with previous biochemical studies (Baur, Minier et al. 2006). The subunit identity is further substantiated by clearly defined glycosylation, as discussed in further detail below. In agreement with the FSEC experiment in which we defined the subunit specificity of the 8E3 Fab, we find that the epitope of the Fab fragment resides entirely on the periphery of the α1 ECDs. While the Fab binding site is near the crucial C-loop that covers the orthosteric binding site, we note that it does not overlap with it and thus is unlikely to directly influence agonist binding, in agreement with the agonist binding studies.

Subunits and subunit interfaces

Subunit-subunit interactions within the extracellular domain play a major role in PLGIC function (Jones and Henderson 2007) and the ECD has also been shown to be important for $GABA_A$ receptor assembly with an interaction area of ~1150 -1750 $Å^2$ (Supplementary Table 2). Five unique subunit interfaces exist in the triheteromeric receptor and to examine the differences in the subunit interfaces, we superimposed the (+)-subunits of subunit pairs (Figure 2). While we observed a similar arrangement of the ECDs at each interface, subtle differences were observed, due to variations in amino acid sequences. When comparing subunit interfaces of β(+)/α*(-) and β*(+)/α(-), we find that similar interactions exist at both these interfaces (Figure 2D and 2E). Similarly, when one compares the interfaces of α*(+)/γ(-) to α(+)/β(-), these two interfaces differ both from each other and in comparison to the β/α interface. The α*(+)/γ(-) interface is less extensive and numerous interactions which are present at other subunit interfaces are lost (Figure 2C).

Neurotransmitter binding sites

Neurotransmitter binding sites in Cys-loop receptors are located at the interface of two adjacent subunits, composed of the three loops from the principle (+) subunit and from β-strands from the complementary (-) side (Nys, Kesters et al. 2013). For the $GABA_A$ receptor used in the studies reported here, saturating GABA leads to maximal activation, similar to the wild-type $GABA_A$ (Supplementary Figure 3A)(Sigel and Steinmann 2012). To determine the molecular basis for GABA binding, we determined the structure of $GABA_A$ receptor in the presence of saturating GABA. To our surprise, we found three visible densities at the approximate position of the neurotransmitter binding sites, at the interface between the β*(+)/α(-), the α(+)/β(-) and the β(+)/α*(-) subunits, an observation

that diverges from previous studies suggesting that there are two canonical GABA binding sites at the β*(+)/α(-) and β(+)/α*(-) interfaces (Figure 3C and Supplementary Figure 7) (Chua and Chebib 2017). Nevertheless, we note that some studies have pointed out that GABA may bind to other interfaces besides the two canonical sites (Chua and Chebib 2017). The oval-like densities in the two canonical sites were assigned to GABA; the density feature at the β(+)/α*(-) interface is weaker than that at the β*(+)/α(-) yet we nevertheless believe that these features are reasonably well fit by GABA molecules. Interestingly, the third density feature at the α(+)/β(-) interface, with a sausage-like shape, has the strongest density. Because GABA is the only small molecule present in the sample buffer that has a size and shape similar to the density feature, we believe that the density is likely a bound GABA molecule. Further studies will be required to experimentally determine GABA binding stoichiometry and higher resolution cryo-EM studies will be needed to more thoroughly define the density features.

In the canonical binding sites, GABA wedges between the β*(+) and α(-) subunits with its amino group sandwiched between Tyr230 and Tyr182 on the β*(+) side, and Arg93 on the α(-) side, also making contact with carbonyl oxygen groups. The amino-group of GABA is likely stabilized by cation-π interaction with Tyr182, hydrogen bonds with Glu180 (loop B) and backbone carbonyl oxygen of Tyr182 (loop B) side, while carboxylate group of GABA forms a salt bridge with Arg93 (β2 strand) (Figure 3A). Similar neurotransmitter binding interactions have been previously reported in the other Cys-loop members, such as GluCl and GlyR (Hibbs and Gouaux 2011, Du, Lu et al. 2015). Superimposing this canonical binding site with the putative third GABA binding site in the interface of α(+)/β(-), the important interaction residues are largely invariant, except for

Gly184 taking place of Glu182 and Gln89 taking place of Arg93. Cation- π interactions stabilize the amino group of GABA, whereas the carboxylate oxygen group of GABA makes a contact with Thr233 in loop C, which is in a more “closed” form in the third GABA binding site (Figure 3C), in accord with the central concept that loop C switches from open to closed when agonist is bound.

We also superposed the γ(+)/β(-) and α*(+)/γ(-) sites with the canonical GABA binding interface β*(+)/α(-), finding major differences among the residues that play important roles in binding GABA, differences that probably lead to weak or no GABA binding (Figure 3D and E). In inspecting these sites that include the γ subunit, we have attempted to better understand the binding site of diazepam, an allosteric modulator of γ-subunit containing $GABA_A$ receptors which substantially potentiates current in the presence of GABA (Supplementary Figure3) (Li, Eaton et al. 2013). Previous studies demonstrated that diazepam binds to the α*(+)/γ(-) interface with a high affinity (Li, Eaton et al. 2013). Indeed, we find α*His128 could provide a strong aromatic or hydrophobic interaction with the pendant phenyl ring of diazepam. Additionally, α*Tyr236, α*Tyr126, α*Tyr186 and γTyr115 likely contribute to the hydrophobic interaction with diazepam (Figure 3F). All these key structural residues surrounding around the putative diazepam are also identified in the model building and functional experiments (Richter, de Graaf et al. 2012, Wongsamitkul, Maldifassi et al. 2017).

Glycosylation in the extracellular vestibule

A glycosylation site was found at Asn137 of the α subunit, within the extracellular vestibule of the receptor, a site of post translational modification that is distinct from the other $GABA_A$ receptor subunits (Figure 4A) and not observed before in any Cys-loop receptor.

This site is predicted to be glycosylated based on the sequence analysis (Blom, Sicheritz-Ponten et al. 2004, Julenius, Molgaard et al. 2005, Miller and Aricescu 2014). At the same time, the quality of cryo-EM map allowed us to confidently locate the density of the sugar residues involved in glycosylation. For the α subunit at Asn137 have built a carbohydrate chain with 7 sugar residues and for the α* subunit at Asn 137 we have built a carbohydrate chain with 3 sugar groups. These two carbohydrate chains are remarkably well ordered, a feature that is likely due to the fact that the chains are contained within the extracellular vestibule and are in direct contact with numerous protein side chains.

Additional glycosylation sites found in the β subunit have been previously observed in the β3 crystal structure (Miller and Aricescu 2014) and are located on external surface of the receptor, pointing away from the receptor (Figure 4B). The glycosylation at the α subunit is well supported by the density to the extent that even chain branches can be easily defined (Figure 4C and D). This glycosylation sites are located in the ECD at the center of the pore (Figure 4B, E and F). The glycosylation occupies a large portion of the pore in the ECD and there are extensive and apparently specific interactions observed with the γ subunit involving residues Asn139, Lys143 and Trp161 (Figure 4F). We speculate that the glycosylation at Asn 137 of the α subunit could break the pseudo 5-fold symmetry of the receptor and subtly ‘push’ the γ subunit away from the other four subunits.

We propose that the glycosylation at Asn137 of the α subunits is important for subunit assembly, effectively blocking the formation of pentamers with more than two α subunits, due to the fact that there is simply not enough volume within the extracellular vestibule to accommodate more than two carbohydrate chains. Moreover, we speculate

that the contacts between the carbohydrate at position Asn137 of the α subunit and, for example the Trp161 of the γ subunit, favor the inclusion of the γ subunit as the last subunit in formation of the heteropentamer. We further suggest that these carbohydrate chains within the extracellular vestibule may also modulate receptor gating and, perhaps, ion channel permeation and block by ion channel blockers. Indeed, it is highly intriguing that a posttranslational modification such as *N*-linked glycosylation occupies such an important and 'internal' site in a neurotransmitter-gated ion channel.

Conformation and asymmetry of the TMD

In the $GABA_A$ structure, the intrinsic flexibility of TMD or the presence of detergent micelle prevents us from defining accurate positions of residues in each TM helix, especially in the M4 helices. Nevertheless, the density of the M1, M2 and M3 helices is well defined, allowing us to reliably position the helices. We discovered that the presence of α, β and γ subunits appears to disrupt the 5-fold symmetry observed in the homomeric or diheteromeric Cys-loop receptors (Figure 5) (Nys, Kesters et al. 2013, Miller and Aricescu 2014). While the distances between two adjacent subunits are similar, varying from 22 Å to 23 Å, the angles in the pentagon fluctuate substantially, ranging from 95° to 121° (Figure 5A). Looking at the top-down views of five central M2 helices, two α TM2 helices tend to be away from the other three TM helices. Superposition of two β subunits with homomeric β3 $GABA_A$ receptor structure suggests rotations of each TM helix in the $GABA_A$ relative to corresponding TM helix in homomeric β3, further demonstrating the asymmetric structure of the TMD.

The asymmetry in the TMD makes it more complicated to define the open or closed state of our solved structure, as the M2 helices lining the pore in the β and γ subunits

display similar orientation as in the desensitized homomeric β3, yet the α subunits are farther from the pseudo 5-fold axis, enlarging the pore (Figure 5B). In the future, additional $GABA_A$ structures determined under different detergents, lipids or ligand conditions will be important. It will also be important to uncover the underlying mechanism of how an asymmetric TMD might be coupled to the ECD and how an asymmetric ion channel might have unique permeation and gating properties.

Conclusion

Here we elucidate direct visualization of the subunit stoichiometry and subunit arrangement for a heterotrimeric $GABA_A$ receptor. Several studies suggest that $GABA_A$ receptor assembly occurs via defined pathways that limit the receptor diversity (Sarto-Jackson and Sieghart 2008). Nevertheless, precise molecular mechanisms regarding assembly are unknown. Here we speculate that the larger contact areas in the ECD region likely make the formation of β(+)/α(-) interface favorable, thus leading to α/β assembly intermediates, which then transition to $(\alpha/\beta)_2$ intermediates. The crucial glycosylation site on the α subunit at Asn137 makes is such that addition of a third α subunit to form the pentamer is disfavored, due to steric clashes, and that either a β or a γ subunit will be incorporated to complete the heteropentamer (Figure 6). The presence of the glycosylation site at Asn 137 of a subunit may not only play an important role in ion channel assembly, but it may also be important to ion channel gating, permeation, block and modulation.

This is the first direct visualization of the GABA binding site. Interestingly, we also find a very strong density at a noncanonical site at the α*(+)/β(-) interface. We postulate that this density is GABA although it is also possible that it represents a ligand that co-

purified with the receptor. This could be a binding site for agonists or other small molecules that and is involved in regulation of the receptor function. Finally, this structure lays the foundation for future studies directed towards developing novel therapeutic agents that modulate $GABA_A$ receptor.

The structure of $GABA_A$ receptor reveals an asymmetric TMD and points towards a role of asymmetry in the assembly and function of this receptor. Future studies are needed to understand how receptor asymmetry may be involved in mechanisms of activation, assembly or modulation. Nevertheless, the receptor structure presented here not only lays the groundwork for methods to express and elucidate structures of $GABA_A$ receptors, but it also provides new insight into the role of post translational modifications on $GABA_A$ receptor assembly, structure and function.

MATERIALS AND METHODS

Construct description

The full-length rat $GABA_A$ receptor subunit isoforms α1 (GeneID 29705) and γ2S (GeneID 29709) with the native signal sequence were a gift from Dr. David S. Weiss. The α1-LT construct was generated by removing M3/M4 cytoplasmic loop, residues A342-P408, mutating Y341 to Thr and adding a thrombin site and a His_8 tag to the C-terminus. The β1-LT subunit (GeneID 25450) was synthesized and cloned into pEGBacMam by Bio Basic Inc with residues K334-K439 replaced with Gly-Thr linker, along with a thrombin site and a His_8 tag at the C-terminus. A bicistronic construct containing α1-LT and β1-LT, in the context of the pEG BacMam vector, was used for large scale expression. The γ2S subunit construct has a three residue (Gly-Arg-Ala) insertion between Asp412 and Cys413 along with a thrombin site, a His_8 tag and a 1D4 tag at the C-terminus. For electrophysiology experiments the FusionRed fluorophore was inserted in the γ2S subunit within the M3/M4 loop using an AscI restriction site. A cartoon depiction of all the constructs used is provided in supplementary Figure1.

α subunit specific Fab generation

Purified α1, β1LT receptor complex in L-MNG was used for immunization. Initial screening returned a large number (>200) IgG positive mAb candidates. ELISA screening was used to determine the highest binding antibodies against receptor in the native and denatured states at a 1:300 dilution. Those that selectively bound to the native state were chosen for further characterization. Subsequent ELISA binding results at a 1:3000 dilution further filtered the candidate pool to 40 supernatants which were examined by western dot blot. Subsequent FSEC analysis identified 8E3 as a α1 specific antibody. Isolated mAB at 0.5

mg/ml in 50mM $NaPO_4$ pH 7 buffer containing 10 mM EDTA, 10 mM L-Cys, 1:100 papain (w/w) was digested for 2 hrs at 37 °C. The reaction was quenched by adding 30 mM Idoacetamide and placing on ice for 20 mins in the dark. Post verification of the digestion by SDS page the Fc portion was separated using Protein A resin the flow through containing Fab was collected and concentrated for further use.

Expression and purification

P1 virus for the bicistronic construct and the γ2S subunit was generated and amplified using standard procedures to obtain P2 virus. Viruses were stored at 4 °C in the dark supplemented with 1% FBS. Virus titer was determined using flow cytometry in a ViroCyt Virus Counter 2100 (Ferris, Stepp et al. 2011). The triheteromer was expressed in TSA201 suspension cells. Infection was performed at a cell density of 1.5-3x10^6 cells/mL in Gibco Freestyle 293 Expression medium supplemented with 1% FBS and placed in a humidity- and CO_2-controlled incubator. The total volume of virus added was less than 10% of the culture volume in all cases. Cells were infected with an MOI of 2 for the bicistronic α1-LT and β1-LT virus and the monocistronic γ2S virus. After 24 hrs of infection at 30 °C, sodium butyrate and picrotoxinin were added at final concentrations of 10 mM and 12.5 μM, respectively, and the flasks were shifted 27 °C for another 24 hrs. All procedures hereafter were done either on ice or in a cold room. Cells were harvested by centrifugation and the pellets were washed with TBS pH 8 containing 25 mM $MgCl_2$ and 5 mM $CaCl_2$. The pellets were re-suspended in 30 mL/L of culture volume in wash buffer with 1 mM PMSF, 1X protease inhibitors (leupeptin, pepstatin and aprotinin), 1.5 mM GABA, 20 μM ivermectin, and 25 μg/mL DNase I. Cells were then sonicated for a 3:30 min cycle (15 sec on/off) while stirring. Cell debris were removed by centrifugation at 7500

G for 20 mins, followed by centrifugation at 125000 G for 1.5 hrs, to pellet the cellular membranes. Membranes were re-suspended (~ 7 ml/lit culture) in 20 mM $NaPO_4$ pH 8, 200 mM NaCl, 1 mM $MgCl_2$, 1 mM $CaCl_2$, 5 µg/mL DNAse I, 0.3 mM PMSF, 1.5 mM GABA and 10 µM IVM and mechanically homogenized. Membranes were solubilized by adding 2% (w/v) C12M and 1 mM CHS for 1 hr at 4 °C. Solubilized membranes were centrifuged for 50 min at 125000 g. The supernatant was then mixed with 1D4 affinity resin equilibrated in 20 mM $NaPO_4$ pH 8, 200 mM NaCl, 1 mM C12M for 3-4 hrs at 4 °C with gentle mixing. The resin was washed with 100 column volumes of the equilibration buffer; elution was achieved using a buffer supplemented with 0.2 mM 1D4 peptide. The eluted protein was concentrated by ultrafiltration, followed by the addition of 2.1 molar fold excess of 8E3 Fab. The concentrated sample was loaded onto a Superose 6 increase 10/300 GL column equilibrated with 20 mM HEPES pH 7.3, 200 mM NaCl, 1 mM C12M and 1.5 mM GABA. The flow rate was kept at 0.5 mL/min.

Radio ligand binding assay

Binding assays were performed with the 10 nM receptor-Fab complex using either 0.75-500 nM [3H]-Muscimol or 1-1000 nM [3H]-Flunitrazepam in a buffer containing 20 mM Tris pH 7.4, 150 mM NaCl, 1 mM DDM, 20 µg/ml BSA and 1 mg/ml YiSi Copper HIS TAG scintillation proximity assay beads (Perkin Elmer, MA). Flunitrazepam binding was measured in the presence of 1.5 mM GABA. Non-specific signal was determined in the presence of 1 mM GABA for the Muscimol and 1 mM Diazepam for Flunitrazepam. Experiments were performed in using triplicate measurements. Data was analyzed using Prism 7.02 software (GraphPad, CA) using one site-specific binding model.

Electrophysiology

TSA-201 cells grown at 30 °C in suspension were transfected with plasmid DNA encoding the bicistronic α1LT/β1LT construct and the monocistronic γ2S-FR construct using Lipofectamine 2000. Cells were plated on glass coverslips 2 hours prior to recording, and all recordings were conducted 18-36 hours after transfection. Individual cells were recorded from only once.

Pipettes were pulled and polished to 2-4 MΩ resistance and filled with internal solution containing (in mM): 140 CsCl, 4 NaCl, 4 $MgCl_2$, 0.5 $CaCl_2$, 5 EGTA, 10 HEPES pH 7.4. Unless otherwise noted, external solutions contained (in mM): 140 NaCl, 5 KCl, 1 $MgCl_2$, 2 $CaCl_2$, 10 Glucose, 10 HEPES pH 7.4. For all electrophysiology experiments requiring Fab, 25 nM Fab was maintained in all bath and perfusion solutions. For potentiation experiments, currents were elicited via step from bath solution to solution supplemented with either 5 μM GABA or 5 μM GABA + 1 μM Diazepam. An unpaired t-test with Welch's correction was used to analyze changes in potentiation with or without Fab. External solution exchange was accomplished using the RSC-160 rapid solution changer (Bio-Logic). Membrane potential was clamped at -60 mV and the Axopatch 200B amplifier was used for data acquisition. All traces were recorded and analyzed using the pClamp 10 software suite.

Cryo-EM data collection

The gold 200 mesh quantifoil 1.2/1.3 grids were covered with a fresh layer of 2 nm carbon using Leica EM ACE600 coater. The grids were glow discharged at 15 mA for 30 s using Pelco easiGlow followed by the application of 4 µL 1 mg/mL PEI (MAX Linear Mw 40k from Polysciences - 24765) dissolved in 25mM HEPES, pH=7.9. After 2 minutes, PEI was removed using filter paper immediately following by two washes with water. The grids

were dried at room temperature for 15 mins. Graphene oxide (Sigma - 763705) at 0.4 mg/mL was centrifuged at 1000 G for 1 min. 4 µL of this was applied to the grids for 2 mins. Excess graphene oxide was blotted away followed by two water washes. The grids were finally dried once again for 15mins at room temperature before use. 2.5 µL of 0.15 mg/mL receptor sample was applied to the shiny side of grids with blot-force of 1 for 2 s using FEI Vitrobot in 100% humidity.

Grids were loaded into a Titan Krios microscope operated at 300 kV. Images were acquired on a Falcon3 direct-detector using counting mode at a nominal magnification of 120,000, corresponding to a pixel size of 0.649 Å and at a defocus range between -1.2 µm to -2.5 µm. Each micrograph was recorded over 200 frames at a dose rate of ~0.6 e−/pixel/s and a total exposure time of 40 s, resulting in total dose of ~37 e−/Å^2.

Cryo-EM data analysis

Beam induced motion was corrected by MotionCor2 (Zheng, Palovcak et al. 2017). The defocus values were estimated by Gctf and particles were automatically picked by DoG-picker (Voss, Yoshioka et al. 2009, Zhang 2016). The extracted bin2 particles were imported to Cryosparc (Punjani, Rubinstein et al. 2017). Two rounds of 2D classification were performed by Cryosparc to remove ‘junk’ particles. The remaining particles were then used to generate an initial model using Cryosparc. The resulting initial model subjected to homogenous refinement using Cryosparc. Particles picked by DoG-picker were also extracted as bin4 particles by Relion followed by 2D classification (Scheres 2012). Good particles from these were selected and re-extracted as bin2 particles followed by another round of 2D classification. 7 of these good class averages were chosen as template for Relion automatic particle picking. These template based

automatically picked particles were extracted as bin2 particles following by two rounds of 2D classification. The particles obtained from these good classes were combined with the particles exported by Cryosparc followed by removing the duplicates using an in-house script. Before performing 3D refinement using Relion, the Gctf generated micrographs star file and Cryosparc generated homogeneous refined map were imported into Relion. The combined bin2 particles were used for 3D refinement in Relion. A mask named receptor-Fv focusing on both the receptor and scFv was generated for the whole map 3D classification and refinement. 3D classification was performed without alignment using 3D refinement generated particle star file. The particles belong to class2 was selected for a final refinement using Relion using receptor-Fv mask. The final map was sharpened using Localscale (Jakobi, Wilmanns et al. 2017). To further refine the ECD region of the receptor, bin1 particles belonging to class2 and class3 were extracted and a mask named ECD-Fv focusing on both the ECD and scFv was created. ECD 3D refinement was performed by applying C1 symmetry. The ECD map was finally sharpened by Relion. Local resolution maps were generated by the command blocres implemented in Bsoft (Heymann and Belnap 2007).

Model building

Homology models for the α1, β1 and γ2 subunit were generated using Swiss-model (Biasini, Bienert et al. 2014). The initial pentameric model was generated with rigid body fitting of the predicted subunit models to the density map using UCSF Chimera (Pettersen, Goddard et al. 2004). The resulting model was manually adjusted in Coot (Emsley and Cowtan 2004), guided by well resolved densities. This model was further refined using phenix_real_space_refine (Adams, Afonine et al. 2010) For the whole map

model, after phenix refinement, map cc between the whole map model and map was 0.787 indicating a good fit between the model and the map. For the ECD map model, the map cc between the map and the entire model was 0.6753. The final model has a good stereochemistry as evaluated by molprobity (Chen, Arendall et al. 2010)(Supplementary Table 1).

ACKNOWLEDGEMENTS

We thank D. Weiss for the gift of $GABA_A$ receptor constructs, Dan Cawley for monoclonal antibody production, all Gouaux and Baconguis lab members for helpful comments, and H. Owen for assistance with manuscript preparation. This research was supported by the NIH to E.G. (E.G. R01 GM100400). E.G. is an Investigator with the Howard Hughes Medical Institute.

AUTHOR CONTRIBUTIONS

D.C. carried out initial construct screening and isolated 8E3 mAb and Fab. S.P. carried out large scale purification, ligand binding experiments and negative stain and cryo-EM. H.Z. performed cryo-EM and carried out reconstructions and model building and refinement. J.Y. carried out receptor expression and cryo-EM reconstructions and model building. The electrophysiology was done by N.Y. All authors contributed to the analysis of the data and the preparation of the manuscript.

AUTHOR INFORMATION

The cryo-EM maps and coordinates for whole map and ECD are available upon request. Correspondence and requests for materials should be addressed to E.G. (gouauxe@ohsu.edu)

REFERENCES

Adams, P. D., et al. (2010). "PHENIX: a comprehensive Python-based system for macromolecular structure solution." Acta Crystallogr D Biol Crystallogr 66(Pt 2): 213-22

Basak, S., et al. (2018). "Cryo-EM structure of 5-HT3A receptor in its resting conformation." Nature Commun. 9: 514.

Baumann, S. W., et al. (2002). "Forced subunit assembly in α1β2γ2 GABAA receptors. Insight into the absolute arrangement." J. Biol. Chem. 277.

Baumann, S. W., et al. (2001). "Subunit arrangement of g-aminobutyric acid type A receptors " J. Biol. Chem. 276: 36275-36280.

Baur, R., et al. (2006). "A GABAA receptor fo defined subunit composition and positioning: concatenation of five subunits." FEBS Lett. 580: 1616-1620.

Biasini, M., et al. (2014). "SWISS-MODEL: modelling protein tertiary and quaternary structure using evolutionary information." Nucleic Acids Res 42(Web Server issue): W252-258.

Blom, N., et al. (2004). "Prediction of post-translational glycosylation and phosphorylation of proteins from the amino acid sequence." Proteomics 4(6): 1633-1649.

Braat, S. and R. F. Kooy (2015). "The GABAA receptor as a therapeutic target for neurodevelopmental disorders." Neuron 86: 1119-1130.

Chang, Y., et al. (1996). "Stoichiometry of a recombinant GABAA receptor." J. Neurosci. 16: 5415-5424.

Chen, V. B., et al. (2010). "MolProbity: all-atom structure validation for macromolecular crystallography." Acta Crystallogr D Biol Crystallogr 66(Pt 1): 12-21.

Chua, H. C. and M. Chebib (2017). "GABAA Receptors and the Diversity in their Structure and Pharmacology." Adv Pharmacol 79: 1-34.

Cymes, G. D. and C. Grosman (2016). "Identifying the elusive link between amino acid sequence and charge selectivity in pentameric ligand-gated ion channels." Proc. Natl. Acad. Sci. USA: E7106–E7115.

Du, J., et al. (2015). "Glycine receptor mechanism elucidated by electron cryo-microscopy." Nature 526: 224-229.

Emsley, P. and K. Cowtan (2004). "Coot: model-building tools for molecular graphics." Acta Crystallogr D Biol Crystallogr 60(Pt 12 Pt 1): 2126-2132.

Farrar, S. J., et al. (1999). "Stoichiometry of a ligand-gated ion channel determined by fluorescence energy transfer." J. Biol. Chem. 274: 10100-10104.

Ferris, M. M., et al. (2011). "Evaluation of the Virus Counter(R) for rapid baculovirus quantitation." J Virol Methods 171(1): 111-116.

Gielen, M. and P. J. Corringer (2018). "The dual-gate model for pentameric ligand-gated ion channels activation and desensitization." J. Physiol. 10: 1873-1902.

Goehring, A., et al. (2014). "Screening and large-scale expression of membrane proteins in mammalian cells for structural studies." Nat. Protoc. 9: 2574-2585.

Hassaine, G., et al. (2014). "X-ray structure of the mouse serotonin 5-HT3 receptor." Nature 512: 276-281.

Hauser, C. A., et al. (1997). "Flunitrazepam has an inverse agonistic effect on recombinant alpha6beta2gamma2-GABAA receptors via a flunitrazepam-binding site." J Biol Chem 272(18): 11723-11727.

Heymann, J. B. and D. M. Belnap (2007). "Bsoft: image processing and molecular modeling for electron microscopy." J Struct Biol 157(1): 3-18.

Hibbs, R. E. and E. Gouaux (2011). "Principles of activation and permeation in an anion-selective Cys-loop receptor." Nature 474: 54-60.

Hilf, R. and R. Dutzler (2008). "X-ray structure of a prokaryotic pentameric ligand-gated ion channel." Nature 452: 375-379.

Hirose, S. (2014). Mutant GABAA receptor subunits in genetic (idiopathic) epilepsy. Progress in Brain Research. K. S. Ortrud. Amsterdam, The Netherlands, Elsevier B.V. 213: 55-85.

Huang, X., et al. (2015). "Crystal structure of human glycine receptor-α3 bound to antagonist strychnine." Nature 526: 277-280.

Jakobi, A. J., et al. (2017). "Model-based local density sharpening of cryo-EM maps." Elife 6.

Johnston, G. A. (2014). "Muscimol as an ionotropic GABA receptor agonist." Neurochem Res 39(10): 1942-1947.

Jones, B. L. and L. P. Henderson (2007). "Trafficking and potential assembly patterns of epsilon-containing GABAA receptors." J Neurochem 103(3): 1258-1271.

Julenius, K., et al. (2005). "Prediction, conservation analysis, and structural characterization of mammalian mucin-type O-glycosylation sites." Glycobiology 15(2): 153-164.

Kawate, T. and E. Gouaux (2006). "Fluorescence-detection size-exclusion chromatography for precrystallization screening of integral membrane proteins." Structure 14: 673-681.

Li, P., et al. (2013). "The benzodiazepine diazepam potentiates responses of alpha1beta2gamma2L gamma-aminobutyric acid type A receptors activated by either gamma-aminobutyric acid or allosteric agonists." Anesthesiology 118(6): 1417-1425.

Lynagh, T. and S. A. Pless (2014). "Principles of agonist recognition in Cys-loop receptors." Frontiers in Physiology 5: 1-12.

MacKenzie, D., et al. (1984). "Localization of binding sites for carboxyl terminal specific anti-rhodopsin monoclonal antibodies using synthetic peptides." Biochemistry 23: 6544-6549.

Miller, P. S. and A. R. Aricescu (2014). "Crystal structure of a human GABAA receptor." Nature 512: 270-275.

Nys, M., et al. (2013). "Structural insights into Cys-loop receptor function and ligand recognition." Biochem. Pharmacol. 86: 1054-1062.

Pettersen, E. F., et al. (2004). "UCSF Chimera--a visualization system for exploratory research and analysis." J Comput Chem 25(13): 1605-1612.

Punjani, A., et al. (2017). "cryoSPARC: algorithms for rapid unsupervised cryo-EM structure determination." Nat Methods 14(3): 290-296.

Richter, L., et al. (2012). "Diazepam-bound GABAA receptor models identify new benzodiazepine binding-site ligands." Nat Chem Biol 8(5): 455-464.

Rudolph, U. and H. Mohler (2014). "GABAA receptor subtypes: Therapeutic potential in Down syndrome, affective disorders, schizophrenia, and autism." Annu. Rev. Pharmacol. Toxicol. 54: 483-507.

Sarto-Jackson, I. and W. Sieghart (2008). "Assembly of GABA(A) receptors (Review)." Mol Membr Biol 25(4): 302-310.

Scheres, S. H. (2012). "RELION: implementation of a Bayesian approach to cryo-EM structure determination." J Struct Biol 180(3): 519-530.

Sigel, E. and M. E. Steinmann (2012). "Structure, function and modulation of GABAA receptors." J. Biol. Chem. 287: 40224-40231.

Sigel, E. and M. E. Steinmann (2012). "Structure, function, and modulation of GABAA receptors." J. Biol. Chem. 287: 40224-40231.

Sine, S. M., et al. (2010). "On the origin of ion selectivity in the Cys-loop receptor family." J. Mol. Neurosci. 40: 70-76.

Thompson, A. J., et al. (2010). "The structural basis of function in Cys-loop receptors." Q. Rev. Biophys. 43: 449-499.

Toyoshima, C. and N. Unwin (1988). "Ion channel of acetylcholine receptor reconstructed from images of postsynaptic membranes." Nature 336: 247-250.

Tretter, V., et al. (1997). "Stoichiometry and assembly of a recombinant GABAA receptor subtype." J. Neurosci. 17: 2728-2737.

Trudell, J. R., et al. (2014). "Alcohol dependence: molecular and behavioral evidence." Trends Pharmacol. Sci. 35: 317-323.

Unwin, N. (1993). "Nicotinic acetylcholine receptor at 9 A resolution." J. Mol. Biol. 229: 1101-1124.

Unwin, N. (2005). "Refined structure of the nicotinic acetylcholine receptor." J. Mol. Biol. 346: 967-989.

Voss, N. R., et al. (2009). "DoG Picker and TiltPicker: software tools to facilitate particle selection in single particle electron microscopy." J Struct Biol 166(2): 205-213.

Walsh, R. M. J., et al. (2018). "Structural principles of distinct assemblies of the human α4β2 nicotinic receptor." Nature 557: 261-265.

Wongsamitkul, N., et al. (2017). "alpha subunits in GABAA receptors are dispensable for GABA and diazepam action." Sci Rep 7(1): 15498.

Wu, C. and D. Sun (2015). "GABA receptors in brain development, function and injury." Metab. Brain Dis. 30: 367-379.

Zhang, K. (2016). "Gctf: Real-time CTF determination and correction." J Struct Biol 193(1): 1-12.

Zheng, S. Q., et al. (2017). "MotionCor2: anisotropic correction of beam-induced motion for improved cryo-electron microscopy." Nat Methods 14(4): 331-332.

FIGURE LEGENDS

Figure 1. Architecture of triheteromeric GABAA receptor. (a) 2D class averages for cryo-EM data of triheteromeric $GABA_A$ receptor. Red arrows indicate 8E3 fab binding to α subunits. (b) Overall architecture of cryo-EM map binding with 8E3 fab viewed parallel to membrane plane. The α, β and γ subunits are colored by light green, salmon and blue. The gray densities contributed by 8E3 fabs are labeled as Fab with Fv and Fc representing variable and constant domains, respectively. Representative transmembrane helixes are pointed out by their names. The glycosylation densities are shown in purple in the top down view. (c) Carbon representation of triheteromeric $GABA_A$ receptor with two representative fabs model viewed parallel to the membrane plane. The ECD and TCD are indicated at the left side of the model. The names of the subunits are marked at the top down view of the model. A black star is used to distinguish the one of the subunits of α and β. (d) Carbon representation of α subunit is shown with the pore axis labeled on its right. Secondary structures and important names are noted. (e) Schematic representation of the subunit arrangement of triheteromeric $GABA_A$ receptor from top down view. The colors are consistent with the colors in (b).

Figure 2. Subunit interfaces. (a) ‘top-down’ view of the α*+/β- subunit interface in the extracellular domain. The region defined by the box is expanded in subsequent panels b-f. (b) The α and β subunits flanking the γ subunit are highlighted by an asterisk. The +/- symbols depict the canonical assignment of subunit arrangement as illustrated in Figure 1b-e. Panel d, e show specific interactions between Arg111 from α subunit at the –interface that interacts with Asp188 and Thr185 from the β subunit at the +interface in the β*+/α- and β+/α* interface. This particular interaction thus needs an aspartic acid and

threonine residue at the + interface and an arginine at the –interface. At any interface with α in the +interface such interactions are absent at the (panel b, c) due to a the substitution of Glu192 instead of the aspartic acid in the alpha subunit's +interface, even though the arginine residue might be present for example in the – interface example in γ i.e Arg135 (panel c). Similarly this interaction is not seen in any of the interfaces with β in the – position due Thr107 in the place of arginine at the corresponding surface. Furthermore in the γ+/β*- interface corresponding threonine and aspartic acid needed in the + face are also replaced by Pro215 and Glu216 respectively.

Figure 3. Neurotransmitter binding sites. (a) View of binding site between β*(+)/α(-) looking parallel to membrane. Dashed line indicate hydrogen bonds and salt bridge. β*(+) and α(-) are colored in salmon and lime respectively. The residues in β*(+) and α(-) and GABA are depicted in salmon, lime and yellow sticks, respectively. (b) Top down view of $GABA_A$ receptor looking from the extracellular side. α and α* are colored in salmon, β and β* are colored in lime, γ is colored in slate. GABA are shown in yellow sphere. (c) Superposition of α(+)/β(-) with β*(+)/α(-). The residues in the β*(+)/α(-) are shown in gray color. Residues in the α(+) and β(-) are shown in red and lime and salmon sticks, respectively. (d) Superposition of γ(+)/β*(-) with β*(+)/α(-). Residues in the β*(+)/α(-) are shown in gray color. Residues in the γ(+) and β*(-) are shown in red and slate and salmon sticks, respectively.(e) Superposition of α*(+)/γ(-) with β*(+)/α(-).Residues in the β*(+)/α(-) are shown in gray color. Residues in the α*(+) and γ(-) are shown in lime and slate sticks, respectively

Figure 4. Glycosylation of $GABA_A$ receptor. (a) Sequence alignment of the rat $GABA_A$ subunits showing the distinct and glycosylation sites locating on ASN 137 of α subunits

which are in red. The corresponding amino acids locates on γ subunit are colored in green. (b) Top down view of triheteromeric CryoEM map. The glycosylation densities locating on α subunits and β subunits are colored in purple. (c) Two views of the density of glycosylation from α* subunit is isolated and fitted with the three sugar molecules. The ASN137 and the name of sugars are labeled. (d) Similar panel to (c), the density of glycosylation on α subunit is isolated and fitted with seven sugar molecules. (e) Carbon representation of the triheteromeric $GABA_A$ viewed from top down view. The glycosylation structures are shown in spheres. (f) Slice view of the glycosylation and its potential interacting amino acids. The glycosylation structures are shown as sticks in purple together with its host chain name labeled, respectively. The potential interacting amino acids locating on γ subunit are shown in sphere with their names labeled in red.

Figure 5. Asymmetry in the TMD. (a) Top-down view of the TMD in the $GABA_A$ receptor from the extracellular side or intracellular looking perpendicular to membrane. α and α* are colored in salmon, β and β* are colored in lime, γ is colored in slate. Center of mass in each subunit was generated by pymol. Dash lines with indicated distance were in Å. The angles between two subunits are indicated. (b) Superposition of the TMD in the $GABA_A$ receptor with homomeric β3 (PDB code: 4cof). The TMD in the homomeric β3 is colored in red.

Figure 6. Conceptual schematic of triheteromeric receptor assembly. Stearic clashes that prevent the formation of homomeric α5 or α3 containing receptors while other combinations are allowed. Individual subunits are marked and shown as circles, the glycosylation in α subunit at position Asn 137 is shown as Y in red.

SUPPLEMENTARY FIGURE LEGENDS

Supplementary Figure1. Representative FSEC traces showing the subunit specificity of 8E3 antibody. Cells expressing various subunit combinations of subunits (a) α1β1 (b) α1β1γ2S (c) α1β2 (d) α1β2 γ2S (e) α6β2γ2S were solubilized and ran on a fluorescent size exclusion chromatography (FSEC) setup either alone (black trace) or with 8E3 Fab (red trace). Shift in FSEC traces confirm that, expression of the alpha1 subunit is required for 8E3 binding.

Supplementary Figure 2. Construct schematic for the various constructs used in this study. Sited of insertion/deletion and the affinity tags are depicted.

Supplementary Figure 3. α1LT/β1LT/γ2S-FR receptor function. (a) Representative whole-cell patch-clamp recording from TSA-201 cells expressing α1LT/β1LT/γ2S-FR receptors activated by 5 μM GABA in the presence or absence of 1 μM Diazepam. (b) Summary of electrophysiology data representing potentiation by 1 μM Diazepam in the presence or absence of 25 nM Fab, n = 6 cells for both experiments. Unpaired t-test with Welch's correction, p = 0.0040 and 95% confidence interval (CI) = -4.861 to -1.466. Midline and error bars represent mean and SEM, respectively. (c) Dose-response data for GABA from TSA-201 cells expressing α1LT/β1LT/γ2S-FR receptors. EC50 = 28.68 μM (95% CI = 21.38-38.49 μM) or 22.51 μM (95% CI = 12.69-39.93 μM) GABA in the presence or absence of 25 nM Fab, respectively. Error bars represent SEM and n = 6 cells for both experiments and. d-e, Saturation binding curve of [^{3}H]Muscimol (d) and [Methyl-^{3}H] Flunitrazepam (e) to α1LT/β1LT/γ2S receptor Fab complexes, plotted result is from a representative experiment. Kd = 109.3 nM (95% CI = 91.76-129.7 nM) or 5.49 nM (95% CI = 4.25 - 7.05 nM) for [^{3}H] Muscimol and [Methyl-^{3}H] Flunitrazepam, respectively. Error bars represent SEM.

Supplementary Figure 4. The work flow processing of CryoEM data analysis of triheteromeric $GABA_A$ receptor data set.

Supplementary Figure 5. CryoEM analysis of triheteromeric data set. (a) Typical micrograph of triheteromeric $GABA_A$ receptor. (b) FSC curves for the whole map and ECD map. The resolution is determined using gold standard FSC standard (ref). Purple and green curves represent for whole map unmasked and masked FSC curve, respectively. The resolution for the unmasked and masked map is 3.8 Å and 3.5 Å, respectively. Red and blue curves represent for the ECD map unmasked and masked FSC curve, respectively. And the resolution for unmasked and masked map is 3.1 Å and 2.7 Å, respectively. (c) and (d) The particle angular distribution for whole map and ECD map, respectively. (e) and (f) The local resolution map for whole map and ECD map, respectively.

Supplementary Figure 6. Representative densities for CryoEM map of triheteromeric $GABA_A$ receptor. (a) Glycosylation density locating on α and α* subuints sitting in the channel of the receptor are shown, respectively. The glycosylation densities at the outside of receptor locating on β subunit are shown. These densities are from ECD map. (b) The representative densities of β3 strand from α, β and γ subunits, and the densities are isolated from ECD map. (c) TM3 and TM4 densities for α, β and γ subunits are isolated from the whole map.

Supplementary Figure 7. Densities surrounding the GABA binding pocket. Three extra densities were found between the interfaces of subunits, (a) for β*(+)/α(-) interface, (b) for α(+)/β(-) interface and (c) for β(+)/α*(-). GABA molecules were placed in these

densites colored with yellow bonds, blue nitrogen and red oxygen. Due to the weak densities, it was hard to determine the exact positions of the GABA molecules.

Supplementary Table 1 legend

Statistics of data collection, 3D reconstruction and models

Supplementary Table 2 legend

Statistics of solvent accessible surface areas

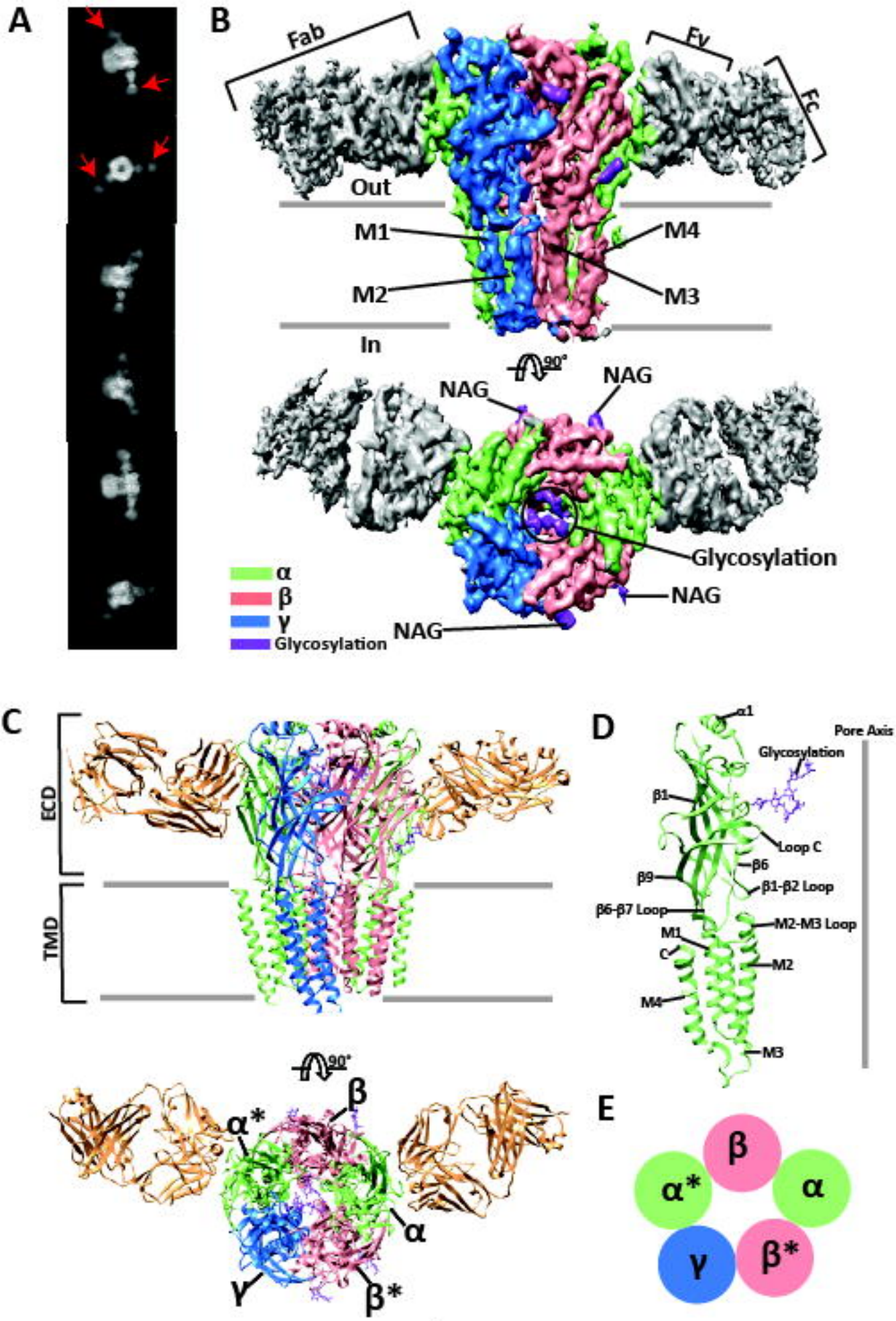
A
B
Fab
Fv
Fc
Out
M1
M4
M2
M3
In
90°
NAG
NAG
Glycosylation
NAG
NAG
α
β
γ
Glycosylation
C
ECD
TMD
90°
β
α*
α
γ
β*
D
α1
Pore Axis
Glycosylation
β1
Loop C
β6
β9
β1-β2 Loop
β6-β7 Loop
M2-M3 Loop
M1
C
M2
M4
M3
E
β
α*
α
γ
β*

Figure 1

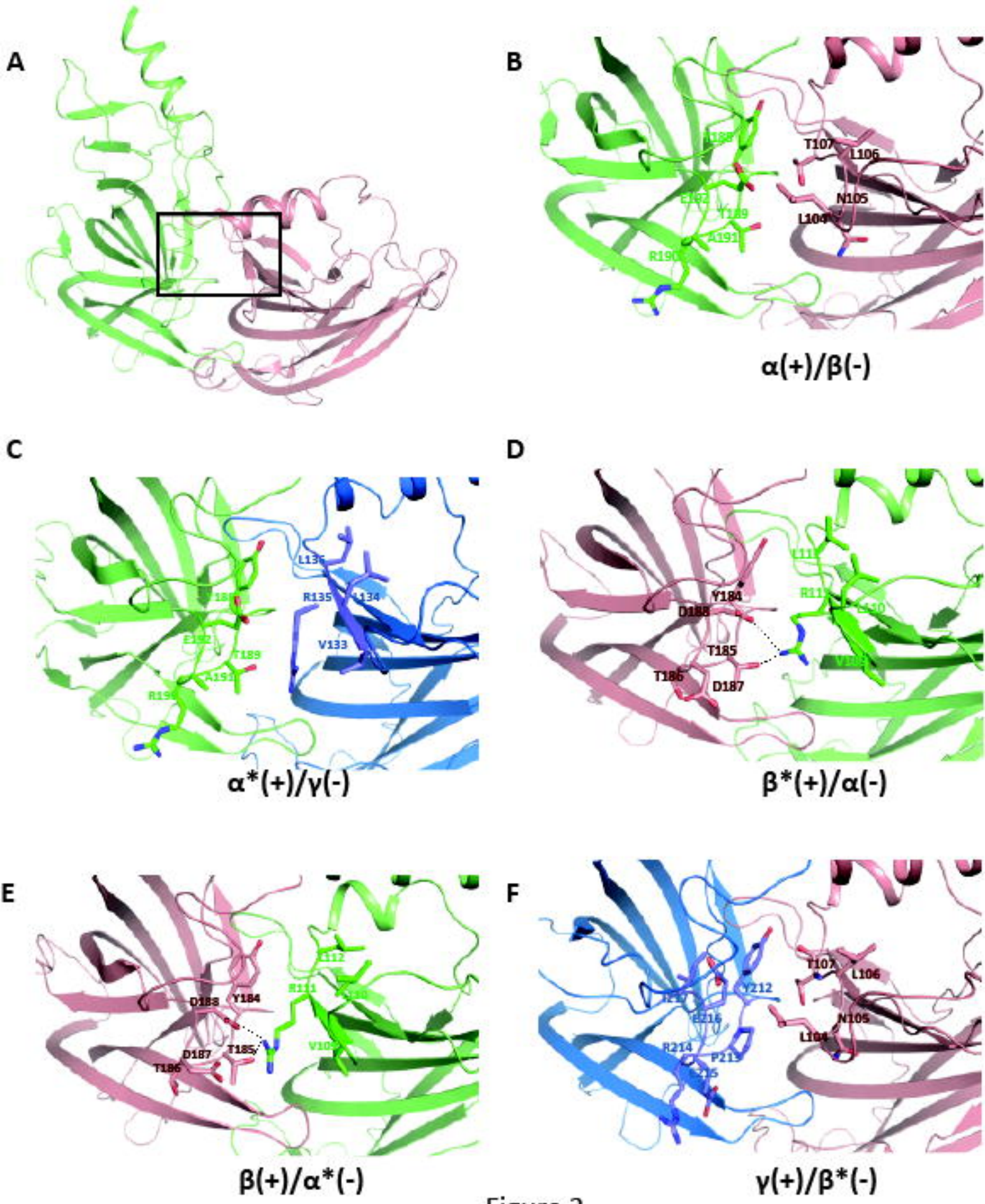
A
B
T107
L106
N105
L104
α(+)/β(-)
C
L135
R135
V133
α*(+)/γ(-)
D
Y184
D188
T185
T186
D187
β*(+)/α(-)
E
D183
Y184
D187
T185
T186
β(+)/α*(-)
F
T107
L106
N105
L104
Y212
R214
P213
γ(+)/β*(-)

Figure 2

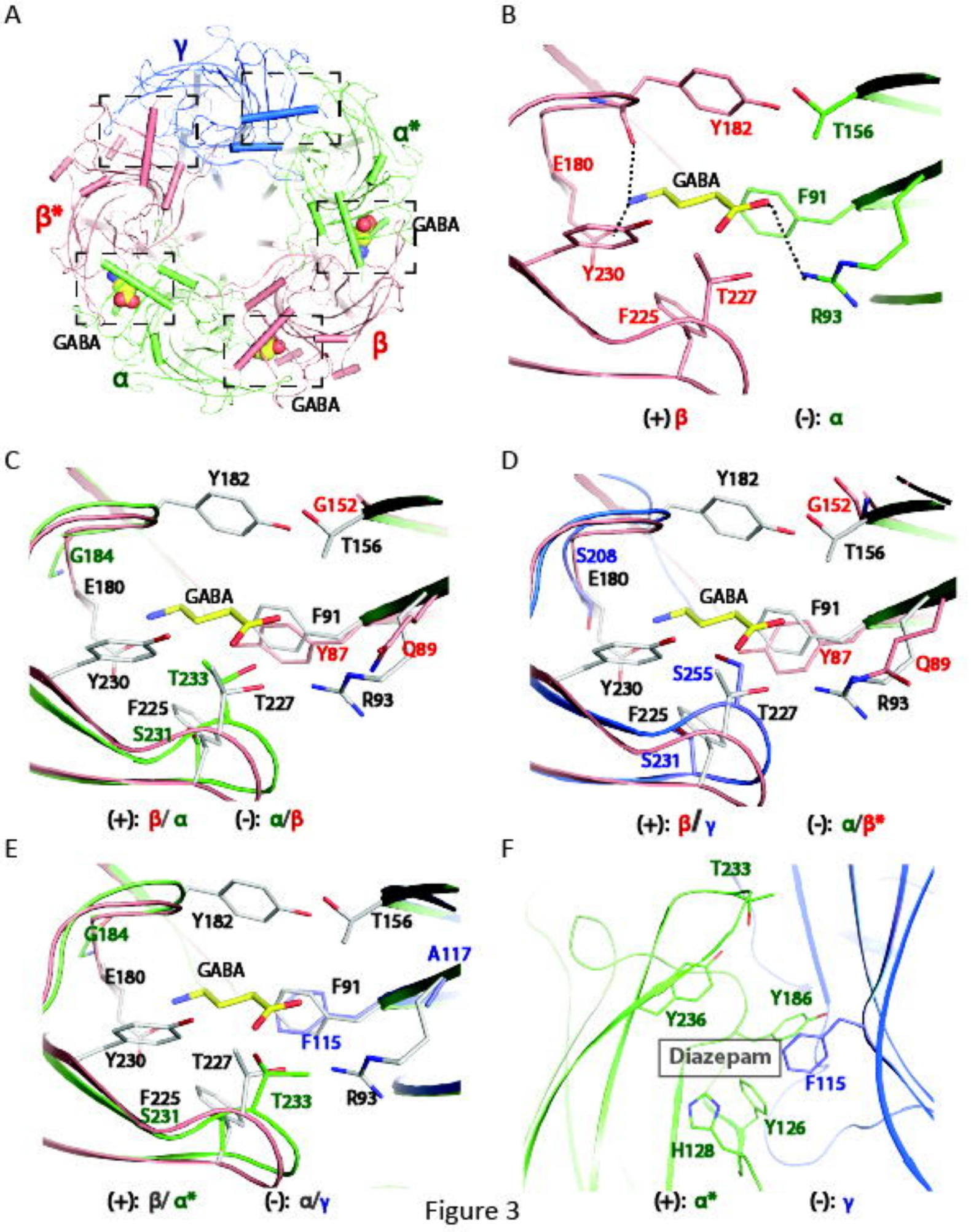
A
γ
α*
β*
GABA
GABA
α
β
GABA
B
Y182
T156
E180
GABA
F91
Y230
T227
F225
R93
(+) β
(-): α
C
Y182
G152
T156
G184
E180
GABA
F91
Y87
Q89
Y230
T233
T227
R93
F225
S231
(+): β/ α
(-): α/β
D
Y182
G152
T156
S208
E180
GABA
F91
Y87
Q89
S255
Y230
T227
R93
F225
S231
(+): β/ γ
(-): α/β*
E
Y182
T156
G184
A117
E180
GABA
F91
F115
Y230
T227
F225
T233
R93
S231
(+): β/ α*
(-): α/γ
F
T233
Y186
Y236
Diazepam
F115
Y126
H128
(+): α*
(-): γ

Figure 3

A

```
sp|P62813|GABA_AR-α1   IWTPDTFFHNGKKSVAHNMTMPNKLLRITEDGTLLYTMRLT 160
sp|P23576|GABA_AR-α2   IWTPDTFFHNGKKSVAHNMTMPNKLLRIQDDGTLLYTMRLT 161
sp|P20236|GABA_AR-α3   IWTPDTFFHNGKKSVAHNMTTPNKLLRLVDNGTLLYTMRLT 186
sp|P28471|GABA_AR-α4   VWTPDTFFRNGKKSVSHNMTAPNKLFRIMRNGTILYTMRLT 167
sp|P19969|GABA_AR-α5   IWTPDTFFHNGKKSIAHNMTTPNKLLRLEDDGTLLYTMRLT 168
sp|P30191|GABA_AR-α6   IWTPDTFFRNGKKSIAHNMTTPNKLFRLMHNGTILYTMRLT 161
sp|P15431|GABA_AR-β1   LWVPDTYFLNDKKSFVHGVTVKNRMIRLHPDGTVLYGLRIT 156
sp|P63138|GABA_AR-β2   LWVPDTYFLNDKKSFVHGVTVKNRMIRLHPDGTVLYGLRIT 155
sp|P63079|GABA_AR-β3   LWVPDTYFLNDKKSFVHGVTVKNRMIRLHPDGTVLYGLRIT 156
sp|P23574|GABA_AR-γ1   IWIPDTFFRNSRKSDAHNITTPNRLLRIWSDGRVLYTLRLT 183
sp|P18508|GABA_AR-γ2   IWIPDTFFRNSKKADAHNITTPNRMLRIWNDGRVLYTLRLT 184
sp|P28473|GABA_AR-γ3   IWIPDTIFRNSKTAEAHNITTPNQLLRIWNDGKILYTLRLT 166
sp|P18506|GABA_AR-δ    LWLPDTFIVNAKSAWFHDVTVENKLIRLQPDGVILYSIRIT 159
sp|Q9ES14|GABA_AR-ε    LWIPDTFFRNSKRTQEYDITIPNQMALIHKDGKVLYTVRMT 191
tr|G3V875|GABA_AR-θ    LWVPDCYFVNSKDAFVHDVTAENRVFQLHPDGTVQYGIRLT 173
sp|O09028|GABA_AR-π    LWVPDTYIVESKKSFLHEVTVGNRLIRLFSNGTVLYALRIT 155
sp|P50572|GABA_AR-ρ1   IWVPDMFFVHSKRSFIHDTTTDNVMLRVQPDGKVLYSLRVT 194
sp|P47742|GABA_AR-ρ2   IWVPDVFFVHSKRSFTHDTTTDNIMLRVFPDGHVLYSMRIT 173
sp|P50573|GABA_AR-ρ3   IWVPDIFFVHSKRSFIHDTTVENIMLRVHPDGNVLFSLRIT 176
```

B

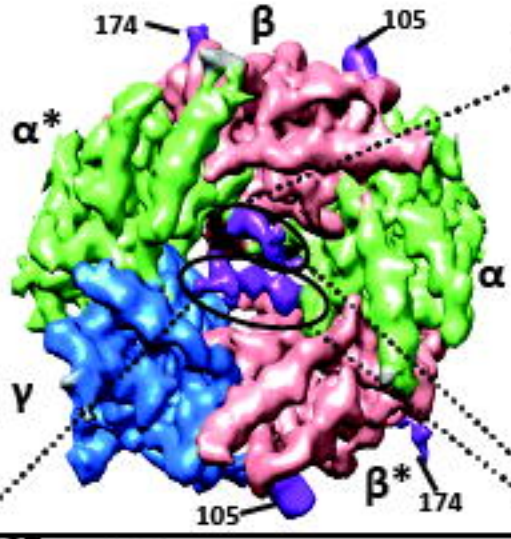

C

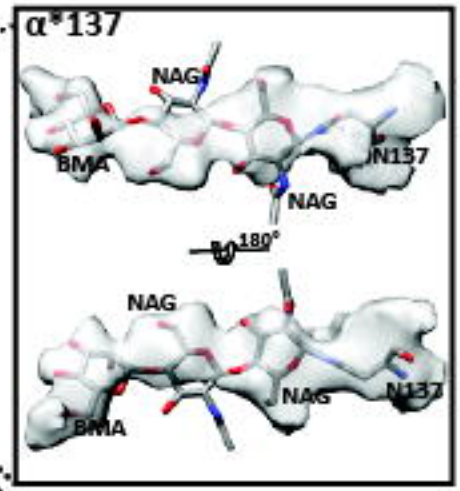

D

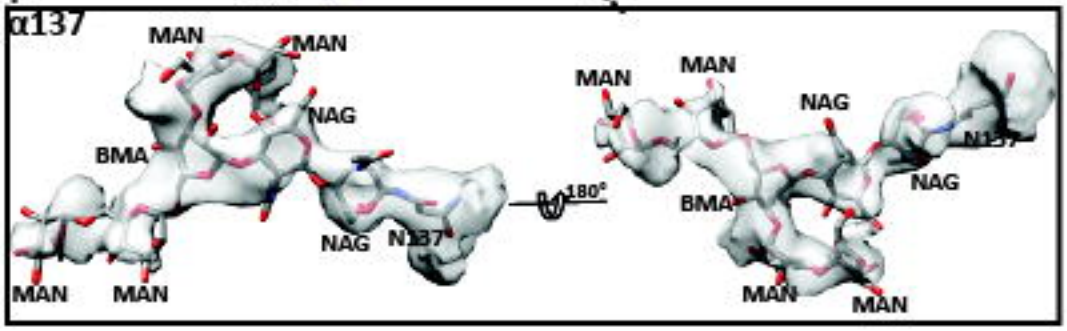

E

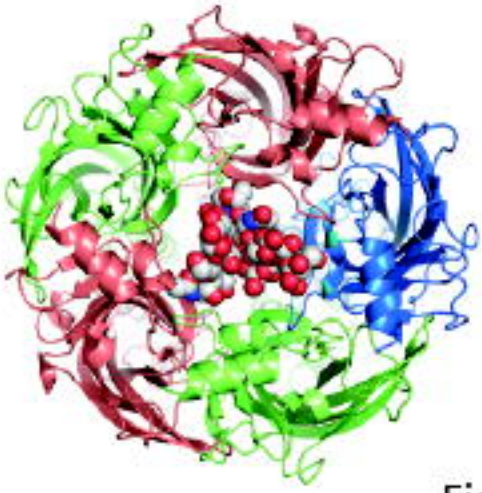

F

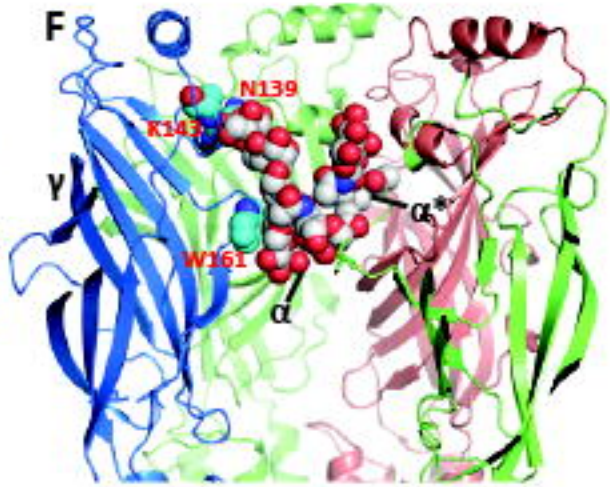

Figure 4

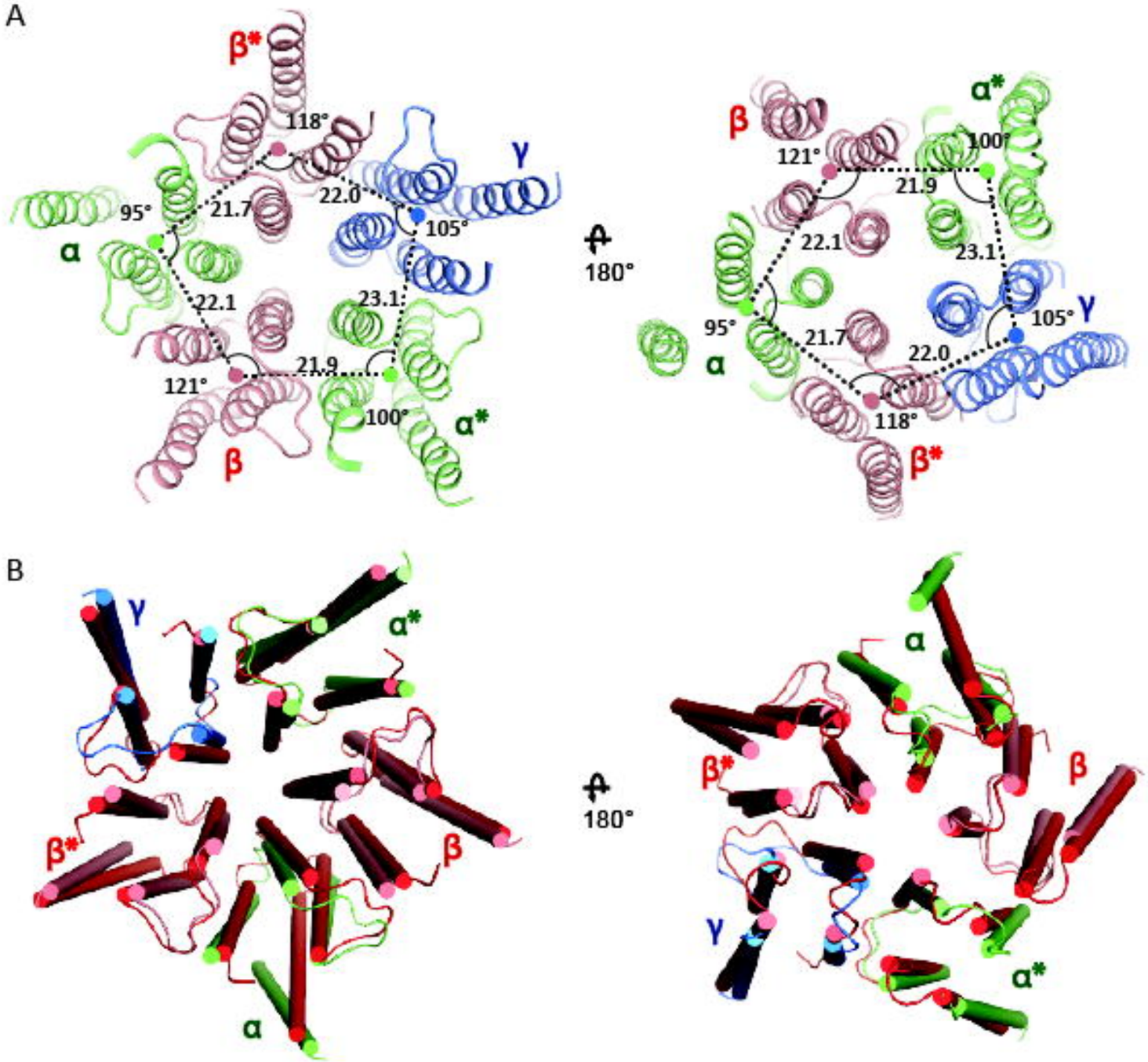
A
β*
118°
γ
95°
21.7
22.0
105°
α
22.1
23.1
21.9
121°
100°
α*
β
180°
β
α*
121°
100°
21.9
22.1
23.1
95°
21.7
22.0
105°
γ
α
118°
β*
B
γ
α*
β*
β
α
180°
α
β*
β
γ
α*

Figure 5

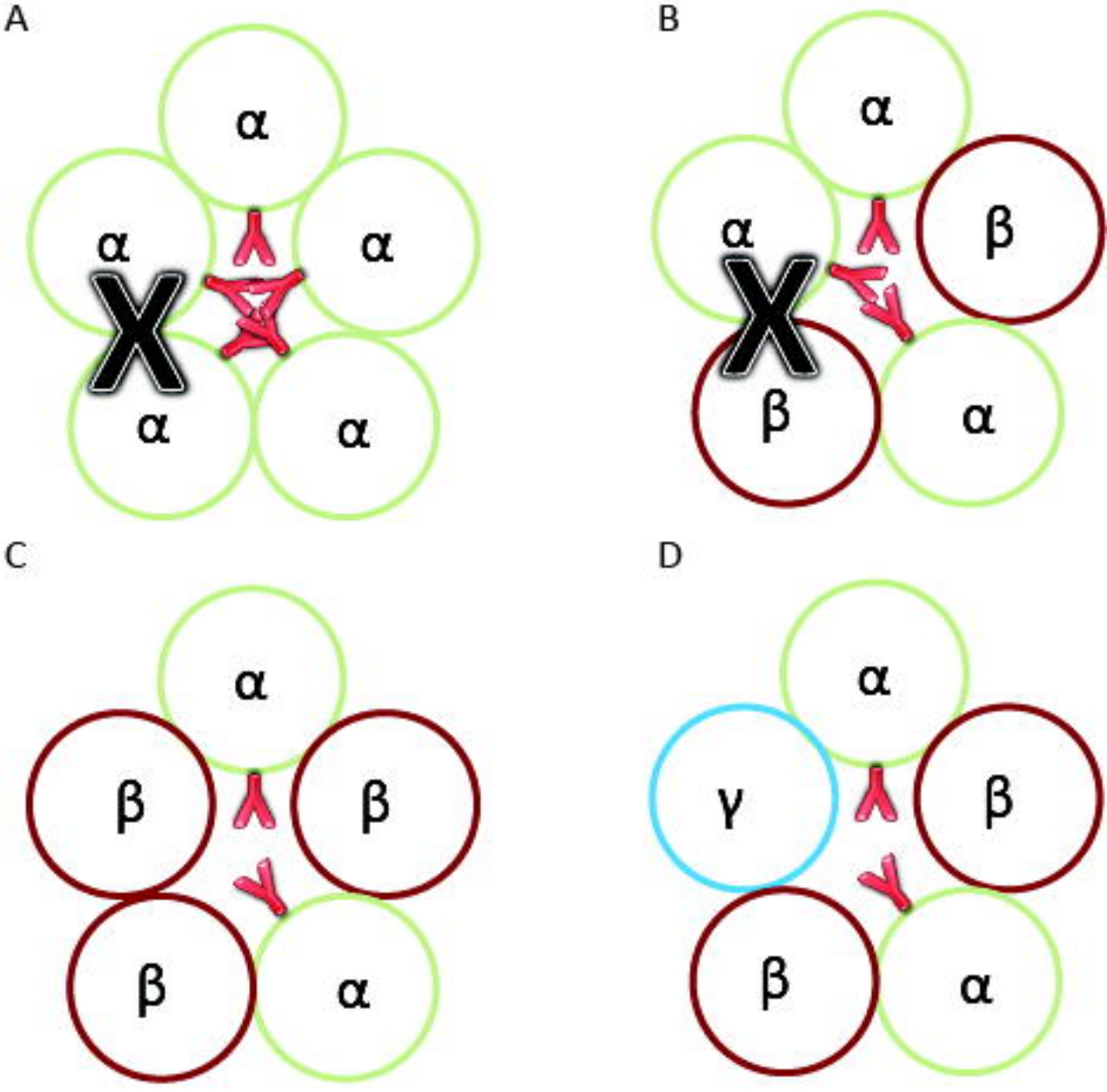

Figure 6